Nanoscale Clustering of RGD Peptides at Surfaces Using Comb Polymers. 2. Surface Segregation of Comb Polymers in Polylactide

Darrell J. Irvine, Anne-Valerie G. Ruzette,† and Anne M. Mayes*

Department of Materials Science and Engineering, Massachusetts Institute of Technology, Cambridge, Massachusetts 02139

Linda G. Griffith

Department of Chemical Engineering & Division of Bioengineering and Environmental Health, Massachusetts Institute of Technology, Cambridge, Massachusetts 02139

Received January 12, 2001; Revised Manuscript Received April 11, 2001

Part 1 of these studies described poly(methyl methacrylate-*r*-polyoxyethylene methacrylate) P(MMA-*r*-POEM) comb polymers that present Arg-Gly-Asp (RGD) peptides at a surface in nanoscale clusters on a protein-resistant background for control of cell adhesion. Here in part 2, we examine surface segregation of these peptide-modified and unmodified comb polymers blended with polylactide (PLA) as a self-assembly approach suitable for surface modification of porous tissue engineering scaffolds. Multiple thermodynamic driving forces for surface enrichment of the comb polymer are exploited by annealing PLA/P(MMA-*r*-POEM) blends above the glass transition of the blend components but below the melting point of PLA, while in contact with water. Predictions of the interfacial composition profiles of annealed blends were made using a self-consistent field (SCF) lattice model. The calculations predict strong enrichment of the comb in the top ∼50 Å of blends, and organization of comb molecules in quasi-2D conformations at the interface, similar to the apparent structure of pure comb surfaces in contact with water described in part 1. Experimentally, PLA/comb blend surfaces were characterized by contact angle measurements, XPS, quantification of ligand-cluster surface density and stability by AFM and fluorescent nanosphere labeling, and cell attachment assays. These data were consistent with SCF predictions, showing significant enrichment of the comb at water-annealed surfaces and RGD cluster densities consistent with 2D conformations for comb molecules in the surface layer. Bulk miscibility of the blends was verified by dynamic rheometry, small-angle neutron scattering, DSC and X-ray diffraction studies. Surface segregation of combs provided tunable cell adhesion on PLA through surface-localized nanoclusters of RGD atop a cell-resistant background.

Introduction

In part 1 of these studies, RGD peptides were clustered at poly(methyl methacrylate-*r*-polyoxyethylene methacrylate) P(MMA-*r*-POEM) comb polymer surfaces by attaching the RGD ligands to multiple side chains of each comb molecule, and mixing these peptide-modified polymers with unmodified combs to vary the total ligand cluster density at the surface of comb films.[1] These nondegradable coatings provide a means for control of cell adhesion through the tailored presentation of nanoclustered RGD peptides to cell surface integrin receptors.[1−4] However, a variety of in vivo biomedical applications would best be addressed by a system with cell-signaling properties and bioresorbability or biodegradability. Examples include targeted drug delivery,[5−7] temporary tissue barriers,[8] and cell delivery scaffolds for gene therapy or tissue engineering.[9−12] For the present studies, we focus on the particular application of tissue engineering scaffolds.

Tissue engineering approaches can be broadly classified into two categories; in vivo synthesis and in vitro synthesis.[8] In vivo synthesis is performed by implanting a bioresorbable scaffold into which cells grow from surrounding tissues, regenerating the lost tissue under the guidance of the scaffold and signals from the environment.[8,13] In vitro synthesis is performed by seeding autologous or donor cells on a scaffold in culture and growing the tissue for a specified time in vitro, followed by implantation of a partly regenerated or finished structure.[8,13] Such approaches are studied for replacement or repair of cartilage,[8] bone,[14] skin,[15−18] nerve,[19−21] kidney,[22] blood vessels,[23] and liver.[24]

Scaffolds used in tissue engineering are three-dimensional structures which provide a template for cell organization, guide cell function, and give protection to the delivered cells (mechanical and/or chemical) from the surrounding tissue over an appropriate time period, while enabling exchange

† Current address: UMR 167, CNRS/ELF−Atochem, 95, rue Danton, B. P. 108, 92303, Levallois-Perret, France.

10.1021/bm015510f CCC: $20.00
Published on Web 05/16/2001

of nutrients and waste products.[8,9,11,19] These devices must not induce an intense or prolonged inflammatory response in vivo and must degrade in a controlled manner without toxic byproducts.[8,25,26] Cell scaffolds used in current research are typically open cell foams or nonwoven fiber meshes with pores ranging from a few tens to several hundreds of micrometers in diameter, depending on the application, with porosities $\geq 95\%$.[9,13,25,27]

To date, one of the most difficult challenges in scaffold design is guiding cell function. One approach for controlling cell function on scaffolds is to provide a protein-resistant surface that guides cell function via immobilized ligands that interact specifically with cell surface receptors, controlling cell response by the amount, type, and spatial distribution of ligand.[10,28] The majority of studies on the fabrication and use of tissue engineering scaffolds have focused on the development of a suitable morphology using a polymer with appropriate bulk properties.[11,12,29−31] Comparatively few studies have been concerned with tailoring the surface of biodegradable materials to combine resistance to nonspecific protein adsorption with biochemical signaling, despite the efficacy of this approach for controlling cell function on model surfaces.[2,32−34] This is due in part to the difficulty in chemically modifying the surface of biodegradable materials in a controlled manner. Synthesis of biodegradable polymers with pendant functional groups is difficult and achieved with poor yield, low functionalities, and/or low molecular weights.[35,36] Black et al. investigated one route to functionalize biodegradable poly(lactide) with peptide ligands by preparing block copolymers of PLA and short (~95 units) end-functionalized poly(ethylene oxide) blocks.[37] Films of this block copolymer exhibited a protein resistant PEO surface layer end-capped with the ligand of interest. As an alternative to direct chemical modification of a biodegradable polymer, Park et al. investigated the use of a solid free-form fabrication process (3DP) to incorporate end-functionalized PEO−PPO−PEO block copolymers into the surface of degradable polylactide devices.[10] PLA devices were modified by "printing" microdroplets of block copolymer solution onto the surface. The printed triblock became permanently entangled with PLA chains at the surface after evaporation of the solvent, creating a cell-resistant surface. To elicit hepatocyte adhesion, the PEO chain ends of the triblock were functionalized with a sugar residue recognized by the hepatocyte asialoglycoprotein receptor. Surfaces presenting the tethered sugar were resistant to nonspecific cell attachment but also did not support strong spreading of hepatocytes. They reasoned that much of the ligand was inaccessible at the surface due either to steric interference from unfunctionalized PEO chains or burial of the ligand within the bulk during the printing process.

To address the issues described above, we explored the use of surface segregation to surface modify polylactide-based devices by blending P(MMA-*r*-POEM) comb polymers with polylactide. PLA has suitable bulk properties for tissue-engineering scaffolds, but, as with most synthetic polymers, elicits uncontrolled cellular responses via adsorbed proteins. In part 1, we showed that the quasi-2D organization of the top molecular layer of comb films controls their surface properties.[1] Thus, recapitulation of this top layer structure through comb surface segregation from a biodegradable matrix might provide control over cell responses on all exterior surfaces of 3D scaffolds. To investigate this hypothesis, a numerical self-consistent mean field (SCF) model of PLA/comb polymer blends was developed to predict the interfacial composition profiles of blends annealed in contact with water. Experimentally, thin film blends of PLA and P(MMA-*r*-POEM) annealed in water were characterized by X-ray photoelectron spectroscopy (XPS), contact angle measurements, atomic force microscopy (AFM) coupled with fluorescent nanosphere labeling, and cell adhesion assays, while blend bulk properties were investigated by X-ray diffraction (XRD), differential scanning calorimetry (DSC), small-angle neutron scattering (SANS), and dynamic rheological measurements. The effects of ligand clustering on the surface were explored by co-segregation of unmodified combs and combs functionalized with multiple RGD peptides per chain. This surface-directed self-assembly approach is shown to provide a practical route to implement nanoscale bioligand patterning on bioresorbable devices having complex three-dimensional shapes.

Numerical Modeling

The SCF model used to investigate the blend/water interface is an extension of the original Scheutjens and Fleer lattice SCF model for polymer adsorption,[38−40] as described in part 1 of these studies.[1] Layer concentration profiles normal to the interface were determined for a system comprising three segmental components of equal size: hydrophobic A segments, hydrophilic B segments, and S units representing water (solvent) molecules. Amphiphilic comb polymers were modeled with backbones of 150 segments of A and four-segment side chains of B spaced evenly along the backbone every seven segments (20 teeth total per comb molecule). Blends were modeled as mixtures of combs with A homopolymer having 1000 segments per chain, representative by molecular weight and chemical composition of the PLA/C1 blends studied experimentally.

Two types of calculations were performed. In hard-wall calculations, blends were confined between an impenetrable layer of *S* at layer 0 and a neutral wall at layer 450, modeling a thin film on a solid substrate. Interactions between system components were accounted for by the magnitude of the Flory−Huggins χ parameters. Since the basic repeat units of the experimental system (lactide, methyl methacrylate, and ethylene oxide) are miscible,[41−44] we set $\chi_{AB} = 0$. Interactions of hydrophobic A segments with water were modeled with $\chi_{AS} = 1.25$; this value provided a best fit to experimental XPS data on water-annealed blends (described below). Interactions between PEO and water were modeled with $\chi_{BS} = 0.4$.[45] Equilibrium layer concentration profiles were calculated as a function of bulk volume fraction of comb (ϕ^{b}_{comb}) and comb molecular weight, keeping side chain length and density constant.

To examine the effects of swelling at comb-enriched blend surfaces, a second set of SCF calculations was made, explicitly including water within the lattice as a single-

Table 1. RGD-functionalized Comb Polymer Physical Data

polymer	base material	peptide linked	μg of peptide/ mg of polymer	peptides/ molecule
C1−RGD1	C1	GRGDSP	50.9	2.1
C2−RGD1	C2	GRGDSPK	12.4	1.7
C2−RGD2	C2	GRGDSPK	16.0	2.2
C2−RGD3	C2	GRGDSPK	26.6	3.6
C2−RGD4	C2	GRGDSPK	40.0	5.4

segment molecule. Reflecting boundary conditions were imposed at layers 0 and 150 of the lattice, with layer 0 as the water-rich side of the interface. The water/polymer interface was initially created as described in part 1, by spatially biasing the initial guess for the segment potentials.[1] A larger value of χ_{AS} (=2.5) was used vs the hard-wall calculations to counterbalance the increased entropy of mixing introduced by including the monomeric solvent explicitly in the calculations. Equilibrium volume fraction profiles were calculated for each component of the system.

Experimental Methods

Materials. Sodium cyanoborohydride, Tween 20 surfactant, diiodomethane, and tritolyl phosphate were obtained from Aldrich. Phosphate-buffered saline pH 7.4 and *N*-(2-hydroxyethyl)piperazine-*N*′-(2-ethanesulfonic acid) (HEPES) buffer pH 7.4 were prepared with distilled water from prepackaged dry packets from Sigma. Poly(L-lactide) (M_n ∼ 80 000−160 000) and poly(D,L-lactide) (M_n ∼ 100 000) were obtained from Sigma. Poly(methyl methacrylate) (PMMA, M_n = 168 000, PDI = 1.07) was purchased from PolySciences. Fluorescent polystyrene nanospheres (yellow-green aldehyde sulfate Fluospheres) with a nominal diameter of 29 nm were obtained from Molecular Probes. All materials were used as received.

Carboxylated P(MMA-*r*-POEM) combs, based on copolymers of methyl methacrylate, hydroxy- poly(oxyethylene methacrylate) (HPOEM, M_n ∼ 360), and poly(oxyethylene methacrylate) (POEM, M_n ∼ 475), were synthesized by free radical polymerization as described in part 1.[1] Two batches of polymer were used for these studies, designated C1 (M_n 25 900, M_w 44 900, 62:18:20 MMA:HPOEM:POEM by weight) and C2 (M_n 93,900, M_w 192,000, 66:16:18 MMA: HPOEM:POEM by weight). RGD peptides (GRGDSP or GRGDSPK) were coupled to C1 and C2 as previously described;[1] the compositions of the functionalized RGD combs are listed in Table 1.

Thin Film Preparation. Cell culture substrates were 30 mm glass dishes (Kontes). Single-crystal silicon wafers (Exsil) and glass coverslips (VWR Scientific) were used for contact angle, XPS, and XRD measurements. Glass and silicon substrates were cleaned by immersion in concentrated sulfuric acid for 2 h, followed by rinsing with distilled deionized water and drying under a dry nitrogen stream. Measurements of film thickness and refractive index were made using a Gaertner ellipsometer operating at 633 nm.

Comb polymer films were prepared by spin-coating 0.01 g/mL chloroform solutions onto silicon substrates at 1000 rpm and drying in vacuo for 24 h at 25 °C, providing films ∼1500 Å thick. Polymer blend thin films were prepared by co-dissolving 2−20 wt % C1 or C2 comb polymer with PLA homopolymer in chloroform at 0.03 g/mL. Solutions were stirred ≈3 h to homogenize and subsequently spin-coated as described above, yielding film thicknesses ranging from 2000−3300 Å. To obtain mechanically resilient thicker films for surface degradation experiments, 80:20 w:w PLA:C2−RGD2 blends were prepared by solvent casting 20 μL of 0.03 g/mL chloroform solutions onto 10 mm glass coverslips. Films were allowed to dry in a hood under a glass cover for 24 h followed by 12 h in vacuo at 25 °C.

To effect surface segregation in blend films, samples were annealed at 70 ± 1 °C in 0.2 μm filtered deionized water for 1−4 days. Aqueous annealing of blend samples was carried out in a sealed water bath with self-regulating temperature control. After annealing, samples for XPS, XRD, and contact angle measurements were dried for 24 h at 25 °C in vacuo. For cell culture experiments, water was aspirated from annealed samples, which were subsequently sterilized under a UV lamp for 30 min and used immediately.

The choice of water annealing temperature was dictated by the need to impart mobility to the polymer chains while avoiding significant hydrolysis of the polyester matrix. Reed and Gilding[46] studied the degradation of PLA as a function of temperature and found that the hydrolysis rate increases rapidly with temperature above T_G (∼60 °C).[47] Samples for measuring weight loss during aqueous annealing were prepared by solvent casting poly(L-lactide)/C1 blends (ϕ^b_{comb} ≈ 0.20) from 0.10 g/mL chloroform solutions on clean glass plates. Samples were dried for 12 h in air and then in vacuo for 24 h at 25 °C. Samples (100−200 mg) ∼1.5 mm thick and 0.57 cm^2 in area were cut from the cast films, immersed in sealed vials containing filtered deionized water, and annealed for 4 days at 70 °C. Mass loss was determined by subsequently drying the films in vacuo at 70 °C until a constant mass was obtained and comparing measured values with the preannealed mass. No statistically significant weight loss (1.36 ± 1.39% measured weight loss) was noted.

For comparison with the water-annealed samples described above, other blend films were cast and annealed in a vacuum at 120 °C for 4 days, quenched to room temperature on large aluminum blocks, and immediately subjected to surface analysis. Vacuum annealing at a higher temperature (200 °C, above the T_m of the matrix) to impart increased chain mobility resulted in thermal degradation of the matrix and sublimation of degradation byproducts.

Blend Sample Preparation for Bulk Measurements. Blend samples for rheology and small-angle neutron scattering (SANS) measurements were prepared by solvent casting co-dissolved polymers (0.10 g/mL in chloroform) onto glass plates resulting in films ∼1 mm thick. The films were dried in vacuo at 100 °C for 3 days and then compression molded for 10 min at 125 °C into ∼25 mm diameter disks. XRD samples were prepared by solvent casting 100 μL of a 0.10 g/mL chloroform solution onto cleaned glass 18 mm diameter coverslips, to obtain films ∼30 μm thick. Samples were covered by shallow glass dishes and dried in a fume hood at 25 °C for 24 h and then in

vacuo at 25 °C for 48 h. Some XRD samples were annealed for 4 days in water as described above.

Dynamic Rheological Measurements. Rheological measurements on the poly(D,L-lactide)/comb polymer blends were conducted with a Rheometric Scientific ARES rheometer operated in a parallel plate geometry with 25 mm plates and 0.5 mm plate gap. Nonstereoregular D,L-polylactide was used to allow determination of PLA/comb miscibility without the complication of crystallization. Dynamic storage (G') and loss (G'') moduli of polymer blends were determined isothermally as a function of angular frequency (10^{-1} rad/s $< \omega <$ 10^5 rad/s). Strains were set at 1% to maintain a linearly elastic response from the materials. Storage and loss moduli measured at multiple temperatures were superimposed about a reference temperature of 140 °C to obtain master curves of rheological response for each blend composition.

SANS Measurements. Small-angle neutron scattering (SANS) measurements on poly(D,L-lactide)/comb polymer blends were made at the National Institute of Standards and Technology on the NG-3 beamline of the Cold Neutron Research Facility. Neutrons of wavelength $\lambda = 6$ Å were used, with resolution $\Delta\lambda/\lambda = 15\%$, and a sample-to-detector distance of 6 m. The available scattering vector range in this configuration is $Q = 0.008-0.08$ Å^{-1}. Scattered intensities were corrected for background and detector noise according to standard procedures and scaled to absolute units (cm^{-1}) using a silica standard. Scattering profiles were obtained at 4 temperatures in 25 °C increments, with 30 min between scans for equilibration after temperature changes.

X-ray Diffraction. Spectra were obtained on a Rigaku powder diffractometer using a rotating anode generator operating at 60 kV/300 mA. Pure poly(L-lactide) and 80:20 w:w poly(L-lactide):C1 blend samples were prepared as described above. XRD spectra were collected for samples as-cast and after 4 days water annealing. Scans were made in a $\theta/2\theta$ geometry for $2\theta = 10-60°$ at 5°/min in 0.02° intervals. Background spectra were collected for empty sample holders and subtracted from the sample data. Percent crystallinity (X_c) was calculated for each sample from the intensity vs 2θ curve based on the relative areas of Bragg reflections vs amorphous signal:[48]

$$X_c = A_{Bragg}/(A_{Bragg} + A_{amorph}) \quad (1)$$

Primary Bragg reflections occurred at $2\theta = 14.6$, 16.6, and 22.3°, in agreement with published values for semicrystalline PLA.[49]

Surface Energy Measurements. Surface energies of PMMA, PLA, and P(MMA-*r*-POEM) were determined from contact angle measurements on spin-coated films. Sessile drop measurements were made by placing a 4 μL drop of one of three different liquids (deionized water, diiodomethane (DIM), or tritolyl phosphate (TP)) on the surface and capturing a video image of the drop (Advanced Surface Technologies, Inc. VCA2000 video contact angle system), from which the contact angle was measured. Four measurements on five samples of each material were performed, yielding the mean contact angles and standard deviations reported in Table 2. Surface energies were calculated from these data using the harmonic mean approximation of Young's equation[50]

Table 2. Sessile Drop Contact Angles on Polymers for Surface Energy Calculations

polymer	water contact angle (deg)	DIM contact angle (deg)	TP contact angle (deg)
PMMA	74 ± 0.8	36 ± 3.4	29 ± 2.8
C1	68 ± 1.4	36 ± 8.2	29 ± 1.3
PLA	73 ± 1.3	54 ± 6.4	49 ± 5.5

Table 3. Liquid Surface Energy Parameters Used for Polymer Surface Energy Calculations[50]

liquid	γ^d (dyn/cm)	γ^p (dyn/cm)	γ (dyn/cm)
water	22.1	50.7	72.8
DIM	44.1	6.7	50.8
TP	39.8	1.1	40.9

$$(1 + \cos\theta_i)(\gamma_i^d + \gamma_i^p) = 4\left(\frac{\gamma_i^d \gamma_s^d}{\gamma_i^d + \gamma_s^d} + \frac{\gamma_i^p \gamma_s^p}{\gamma_i^p + \gamma_s^p}\right) \quad (2)$$

where θ_i is the contact angle of liquid i on the polymer surface, γ_i^d and γ_i^p are the dispersive and polar surface energy components of liquid i, and γ_s^d and γ_s^p are the dispersive and polar surface energy components of the polymer. The two unknowns (γ_s^d and γ_s^p) were solved for using pairs of liquid contact angle measurements and the known surface energies of the liquids,[50] listed in Table 3. (DIM measurements were not used for determination of the comb polymer surface energy, as the comb was partially soluble in this liquid). Using these data, the interfacial tension of each of the blend components with water can be approximately calculated using the known γ_p of the polymers and water according to[50]

$$\gamma_{pw} = \gamma_p + \gamma_w - W_{adh,PW} \approx \gamma_p + \gamma_w - 2(\gamma_p\gamma_w)^{1/2} \quad (3)$$

where $W_{adh,PW}$ is the work of adhesion between the polymer and water, calculated using a geometric mean approximation.[51,52]

X-ray Photoelectron Spectroscopy. Chemical analysis of blend film surfaces was performed using a Surface Science Instruments SSX-100 spectrometer, with an electron takeoff angle of 45 °C relative to the plane of the sample. Low-resolution survey and high-resolution C_{1s} spectra were obtained for each sample. Survey scans over 0−1000 eV binding energy range indicated the presence of C and O as expected with no significant contaminant element peaks. High-resolution C_{1s} spectra were fit by subtracting a linear background and introducing a Gaussian−Lorentzian function to describe peaks for each carbon bonding environment in the samples[53]

$$I(E) = 2A\left[\frac{m\sqrt{\ln 2}}{W\sqrt{\pi}}\exp\left(-4\ln 2\left(\frac{E-E_0}{W}\right)^2\right) + \frac{1-m}{\pi W\left[1+4\left(\frac{E-E_0}{W}\right)^2\right]}\right] \quad (4)$$

where $I(E)$ is the intensity at binding energy E, A is the peak area, E_0 is the peak center, W is the full-width at half-maximum intensity, and m is the Gaussian−Lorentzian mixing ratio (1 = pure Gaussian, 0 = pure Lorentzian). The mixing ratio m was constrained between 0.7 and 1.0 for all fits, a range appropriate to the monochromated Al Kα line shape.[53] Good fits were obtained for peak widths ranging from 1.0 to 1.6 eV. Spectra were deconvoluted using known peak positions of the blend components from the literature as follows:[53,54] hydrocarbon (285 eV), $-C(CH_3)(COO)-$ (285.8 eV), $-CH_2CH_2O-$ (286.5 eV), $-OCH_3$ and $-CH(CH_3)-COO-$ (287.0 eV), and $-(COO)-$ (289.0 eV). Near-surface volume fractions of the comb polymer (ϕ^s_{comb}) were calculated from the relative area contributions of peaks in the deconvoluted spectra and the known molecular structures of the blend components.

To further elucidate the structure of blend surfaces, concentration profiles obtained from SCF calculations were used to model XPS data. The ratio of the area of the ethylene oxide (EO) C_{1s} peak ($-CH_2CH_2O-$) in the blend to that in a pure comb polymer sample is[55]

$$A_{EO-blend}/A_{EO-comb} = \left[1 - \exp\left(\frac{-d}{\lambda_E \cos\theta}\right)\right]\left[\sum_{n=1}^{\infty} x_n \exp\left(\frac{-(n-1)d}{\lambda_E \cos\theta}\right)\right] \quad (5)$$

where the summation is carried out over all atomic planes from the surface into the bulk, d is the average spacing between atomic layers in the sample, λ_E is the photoelectron mean free path (=2.3 ± 0.3 nm for Cu Kα radiation ejecting C_{1s} electrons[56]), x_n is the mole fraction of EO carbon in layer n, and θ is the XPS takeoff angle. SCF concentration profiles were used to provide x_n values with an assumed planar spacing of d = 5 Å, approximately equal to the size of 1 SCF lattice layer. SCF calculations assumed a hard-wall surface (in keeping with the high vacuum environment of XPS), varying χ_{AS} to obtain a best fit to the experimental data. The resulting comb concentration profiles supplied x_n values in (5) to obtain theoretical $A_{EO\ blend}/A_{EO\ comb}$ ratios. Best fits to the XPS $A_{EO\ blend}/A_{EO\ comb}$ data were obtained for χ_{AS} = 1.25.

Peptide Surface Density Determination Via AFM Measurements. GRGDSPK peptide clusters present at the surface of PLA/comb/RGD comb blends were labeled by covalently linking fluorescent nanospheres bearing surface aldehyde groups to the ϵ-amine of the peptide's terminal lysine as described in part 1 of these studies.[1] In brief, fluorescent nanospheres with surface aldehyde groups were covalently linked to peptide clusters by placing the nanosphere suspension (2×10^{13} spheres/mL in HEPES buffer) in contact with surfaces in the presence of sodium cyanoborohydride for 24 h at 4 °C. Unreacted spheres were removed by rinsing with Tween 20 solution (0.3 vol % in PBS). Nanospheres were assumed to label a single cluster at the surface, and labeling was assumed to be quantitative to within 10%.[1] Cluster density at the surface of blends was subsequently determined by imaging nanosphere-labeled surfaces with atomic force microcopy. AFM was performed with a Digital Instruments Dimension3000 using Si_3Ni_4 tapping mode cantilevers. Topographical and phase images were obtained of the surface of labeled films using cantilevers with spring constants of 30−60 N/m and resonant frequencies ~320 kHz. The free vibration amplitude (A_0) of the cantilever near the surface but out of contact was typically ~2.2 V. Scans were made at 1 Hz with 512 × 512 pixel sampling and set points of ~$0.5A_0$. Quantitative determination of label density for a given blend composition was performed by analyzing 8−12 2.5 × 2.5 μm scans taken from two to three different labeled samples. The high-T_g polystyrene nanosphere labels (T_g ~ 100 °C) were well resolved in AFM phase images. AFM phase images were analyzed by first thresholding the data and creating binary black/white images from the original scans. The nanospheres exhibited a large phase contrast with blend surfaces, rendering the binary image insensitive to the exact threshold used. The density of nanospheres in the binary images was determined using NIH Image software. Particles were counted in each image, and the total divided by the analyzed surface area (neglecting holes not probed by the AFM tip) to arrive at the surface density of peptide clusters. Cluster densities were converted to total RGD densities by multiplying by the average number of peptides per cluster for the given RGD comb polymer.[1]

Ligand Loss Measurements of Blend Degradation. To assess the stability of peptide ligand at the surface of segregated PLA/RGD comb polymer blends, a degradation study was carried out to measure the loss of ligand from film surfaces. PLA/C2−RGD2 blends were prepared as described above and annealed 1 day in 70 °C water. Peptides present at the surface were subsequently labeled using fluorescent nanospheres as described above. Labeled blend films were scored and floated off the coverslips onto the surface of a water bath, retrieved with tweezers, and placed in the wells of an opaque 96-well assay plate. Then 300 μL aliquots of phosphate buffered saline (PBS) were added to each well, and the covered 96-well plate was incubated at 37 °C in a closed dark incubator. PBS was added to sample wells as necessary on alternate days to avoid significant change in the PBS volume due to evaporation. Every 7 days, PBS was aspirated from the sample wells, samples were rinsed once with 300 μL PBS and aspirated, 300 μL fresh PBS was added, and fluorescence of the samples in the plate was measured using a Molecular Devices SpectraMax Gemini fluorescence plate reader. A standard curve of fluorescence vs nanosphere number was prepared from standard dilutions of nanospheres. Percent label lost over the course of 8 weeks was calculated with respect to the initial average number present.

Cell Attachment Assay. WTNR6 fibroblasts (cell passages 16−26) were cultured in serum-containing media as described in part 1.[1] Fibroblasts to be seeded on samples were grown near confluence in T75 flasks, then suspended using 10× trypsin−EDTA solution (Gibco). Cell concentrations were determined using a Coulter cell counter and diluted appropriately in serum-containing medium to seed surfaces. Tissue culture polystyrene (TCPS, Corning Costar) was used as a control substrate in all cell experiments to monitor for irregularities in media or cell passages. Cell numbers on polymer surfaces were quantified by a fluores-

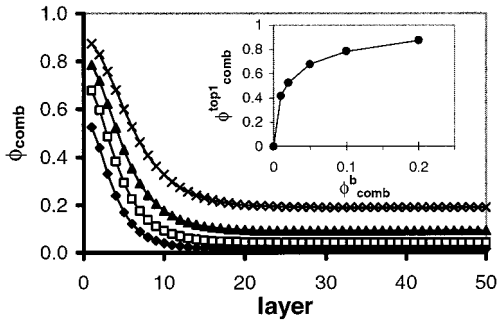

Figure 1. SCF predictions of P(MMA-*r*-POEM) surface segregation in polylactide. (Main figure) Equilibrium comb volume fraction profiles for comb/PLA blends in contact with water at layer 0 (hard-wall approximation). ϕ^{b}_{comb} in each case is (◆) 0.02, (□) 0.05, (▲) 0.10, and (×) 0.20. (Inset) Top surface layer comb volume fractions for each of the bulk comb concentrations plotted in the main figure.

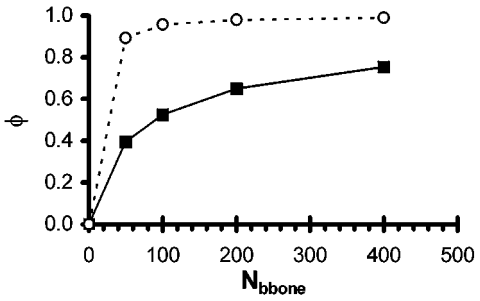

Figure 2. Predicted effect of comb polymer molecular weight on surface segregation in PLA/P(MMA-*r*-POEM) blends: (■) $\langle\phi^{top10}{}_{comb}\rangle$; (○) $\phi^{top1}{}_{comb}$.

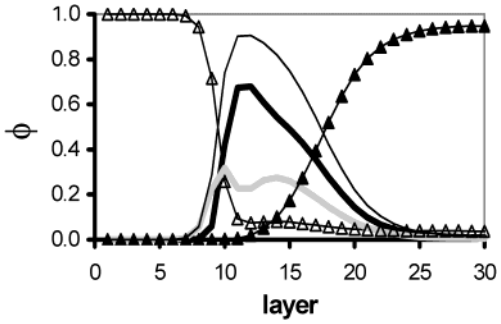

Figure 3. SCF prediction of blend surface swelling by equilibration in contact with water for $\phi^{b}_{comb} = 0.015$. Curves depict the volume fraction profiles of each component: (△) water, (▲) matrix, (—) comb, (—) comb backbone units, (═) comb side chain units.

cent DNA probe assay (CyQuant, Molecular Probes) as described in part 1.[1] In brief, attached cells were lysed with a detergent buffer and mixed with a proprietary fluorescent probe that shows strong emission enhancement on binding DNA. Standard curves correlating sample fluorescence with cell number were prepared for each experiment using standards of known cell density from Coulter counter measurements. Fibroblast attachment to surface-segregated blend thin films was assayed by culturing cells on surfaces for 24 h followed by counting the fraction that adhered. Cell number for each sample was calculated from three independent aliquots of the cell lysate/probe solution. Cell number, surface densities, and % seeded cells adhered are reported as mean values of three to five samples ± standard error.

Results and Discussion

SCF Predictions. Previous SCF studies on comb/linear polymer mixtures predicted surface enrichment of combs even in the absence of preferential enthalpic interactions, due to entropic driving forces derived from the comb architecture.[57,58] Further enrichment might be expected in our experimental system by annealing blends in contact with water, driven by favorable enthalpic interactions of PEO with water and minimization of the hydrophobic effect at the blend surface. Accounting for favorable water-PEO contacts, Figure 1 shows the predicted concentration profiles of PLA/C1 blends in equilibrium with pure water at layer 0 for $\chi_{AS} = 1.25$. The inset plots volume fraction of comb copolymer localized in the topmost surface layer ($\phi^{top1}{}_{comb}$, ~5 Å deep) as a function of bulk comb volume fraction ϕ^{b}_{comb}. The model predicts a strong surface localization of the comb: bulk concentrations of only 10 vol % provide a comb concentration in the surface layer of 80 vol %, and a large excess within the top ~50 Å of the blend.

These calculations were made for a comb polymer having N_{bbone} (segments in the backbone) = 150; for P(MMA-*r*-POEM) comb polymers of equivalent architecture, this corresponds to a molecular weight of approximately 25 000. Previous SCF calculations predicted a strong dependence of comb surface excess on molecular weight (keeping side chain length and density constant) for entropically driven segregation.[57] A significant molecular weight effect is also predicted here, and provides a handle by which comb surface enrichment can be considerably increased. Figure 2 shows the change in $\phi^{top1}{}_{comb}$ and $\langle\phi^{top10}{}_{comb}\rangle$ (the average ϕ_{comb} in the top 10 layers of the blend) for $\phi^{b}_{comb} = 0.10$ with increasing N_{bbone}. Increasing N_{bbone} from 100 to 400 gives rise to an increase in $\langle\phi^{top10}{}_{comb}\rangle$ of about 40%. Although we might expect further modest increases in $\langle\phi^{top10}{}_{comb}\rangle$ up to molecular weights of several hundred thousand, slower kinetics of diffusion for higher molecular weight chains become a practical limitation to achieving the predicted surface enrichment. Comb molecular weights in the range of 25−100K ($N_{bbone} \approx 150-650$ units in our calculations) should provide high surface coverage within a time scale practical for application.

Further SCF calculations were made to examine the effect of water absorption in the blend surface layers, by explicitly introducing water as a single-segment molecule and considering only the interfacial region of the blend. An example of the predicted equilibrium structure of a water/blend interface is shown in Figure 3, for $\phi^{b}_{comb} = 0.015$. Significant swelling of the surface layers is predicted due to enrichment of the amphiphilic comb. The concentration profile of the comb backbone segments peaks in two layers at the interface; side chains depleted from these layers extend into the solvent. The top few molecular layers of the surface are thus composed almost entirely of hydrophilic side chain units and water. This segregation of the hydrophilic and hydrophobic components of combs at the surface is consistent with a quasi-2D arrangement of combs in the surface layer.[1] To obtain this intramolecular segregation, combs in the top molecular layer of the blend have their backbones confined in quasi-2D, weakly interpenetrated conformations in the

plane of the interface. The backbone-rich planes anchor a brush layer of the side chains extending into solution, similar to the top-layer structure predicted by SCF in part 1 of these studies for pure comb polymer films contacting water. Chains in this top layer should thus be organized as disklike objects, meaning that an area of size R_G^2 contains only ~1 comb molecule in the surface layer. This predicted organization would allow efficient presentation of all peptides tethered to combs confined in the surface layer. The similarity in the predicted concentration profiles of comb segments in the topmost surface layers of pure comb films (from part 1) and the surface-segregated combs in these calculations supports the idea that surface-segregated blends should exhibit cell responses comparable to pure comb films.

Blend Miscibility. To avoid bulk phase separation and an accompanying degradation of mechanical properties,[59] a miscible surface-segregated blend is desirable, i.e., a blend that contains a surface layer enriched in cell-guiding comb polymer but remains homogeneously mixed in the bulk amorphous phase of PLA. Experimental determination of the miscibility of semicrystalline poly(L-lactide) with other polymers is made challenging by the inherent phase separation of crystalline and amorphous regions, which confuses attempts to elucidate mixing of a second component in the amorphous phase. We thus carried out miscibility analyses using the nonstereoregular isoform of PLA, poly(D,L-lactide), which does not crystallize and allows a clear determination of miscibility between the polyester and a second component. Bulk miscibility of PLA and the comb polymer was assessed for PLA/C1 blends with dynamic rheological testing and SANS measurements on melt-pressed blend samples. Miscibility of the comb polymer with PLA could not be determined by thermal analysis, as the glass transitions of the comb (T_g = 43 °C)[60] and PLA (T_g = 57 °C) are too close to effectively resolve in blends, especially in light of the broadening of the glass transition which is typically observed in miscible blends.[61]

In rheological measurements, the time−temperature superposition (tTS) principle empirically relates the frequency (ω) dependence of the complex dynamic modulus (G^*) of a material observed at temperature T to that at a given reference temperature according to[62]

$$G^*(\omega,T) = b_T G^*(\omega a_T, T_{ref}) \quad (6)$$

The modulus-scale shift factor b_T and frequency-scale shift factor a_T allow superposition of data at temperature T to a reference temperature (here, T_{ref} = 140 °C). Figure 4a shows tTS master curves for a 50:50 w:w PLA:C1 blend. Qualitatively, the data show a single plateau in the storage modulus and one break in slope moving from high to low frequency, indicative of flow in a homogeneous blend. In contrast, immiscible blends show a second plateau in G' at low frequency due to a long time relaxation mechanism present in phase-separated microstructures.[63] Figure 4 shows a Han plot[64,65] of the 50:50 blend data. Two criteria for a fully homogeneous blend are temperature independence of the log G' vs log G'' curves and a terminal slope approaching 2; both requirements are met by the PLA/comb blend. Similar rheological measurements on 80:20 and 90:10 w:w PLA:C1 blends indicate full miscibility of the polymers over this composition range.

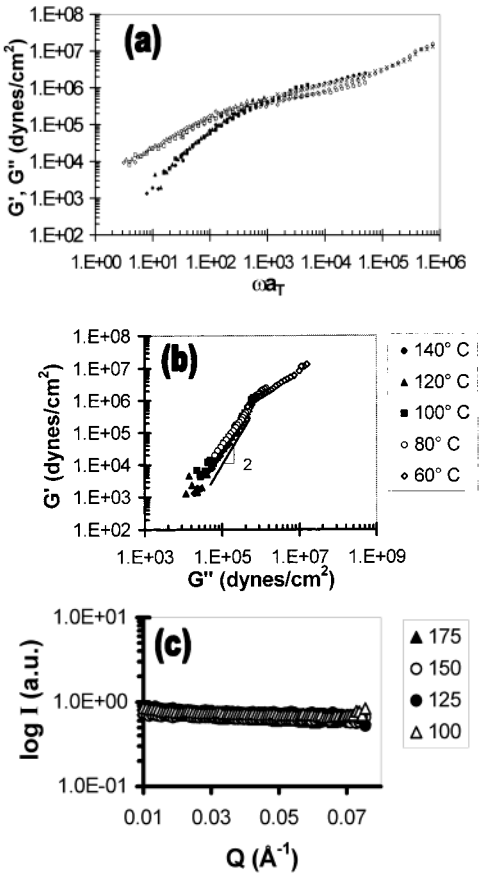

Figure 4. Blend miscibility assessment. (a) tTS master curves for a 50:50 w:w poly(D,L-lactide)/C1 blend from dynamic rheological measurements. Data were taken in 20° increments from 140° to 60 °C. G' open symbols, G'' solid symbols. (b) Han plot of rheological data for the 50:50 PLA:C1 blend. (c) Scattering results for SANS measurements on 90:10 PLA:C1 blends at several temperatures.

Table 4. Measured Surface Energies of PMMA, P(MMA-*r*-POEM), and PLA

polymer	γ^d_p (dyn/cm)	γ^p_p (dyn/cm)	γ_p (dyn/cm)	γ_{pw} (dyn/cm)
PMMA	33 ± 0.6	12 ± 1.5	45 ± 1.6	3.3 ± 1.0
C1	33 ± 0.4	15 ± 0.6	48 ± 0.7	2.6 ± 0.2
PLA	26 ± 1.7	13 ± 4.4	38 ± 4.7	5.6 ± 1.8

Further confirmation of the compatibility of PLA with the comb polymer was provided by SANS measurements made on melt-pressed bulk 80:20 and 90:10 w:w poly(D,L-lactide): C1 blends. Phase separation gives rise to Porod scattering[66,67] from interphase boundaries at low Q, with intensity scaling as Q^{-4}. (The scattering vector $Q = 4\pi\lambda^{-1}\sin\theta$, where λ is the wavelength of the incident neutrons and θ is the scattering angle.) Scattering profiles for the 90:10 PLA:C1 blend are shown in Figure 4c. The samples show essentially background intensity over the entire scattering vector (Q) range examined, again indicating complete miscibility. Similar results were obtained for 80:20 blends.

Surface Energy Measurements of Blend Components. Surface energies of PMMA, C1 comb polymer, and poly(L-lactide) calculated from contact angle measurements are listed in Table 4. As seen previously,[68] introduction of the hydrophilic PEO side chains in the comb polymer raises its

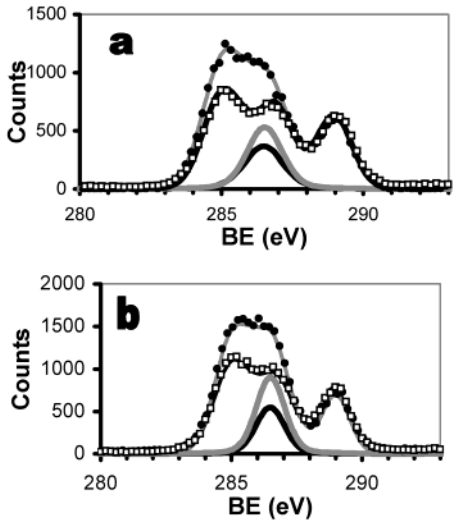

Figure 5. C_{1s} XPS data for PLA/C1 blends: (□) unannealed blend raw counts, (●) annealed blend raw counts, (═) annealed (gray line) blend total fit and EO carbon 1s peak, and (—) unannealed (black line) blend total fit and EO carbon 1s peak. Key: (a) 90:10 w:w PLA:C1. (b) 80:20 PLA:C1.

surface energy (in air) relative to pure PMMA. The measured surface energy of PLA is significantly lower than previously reported from experiments using an underwater contact angle method.[69] This discrepancy could be explained by substantial surface crystallinity or adsorption of oils at the water−polymer interface in the previous study, both of which can substantially increase the measured surface energy.[50] As measured here, PLA shows a surface energy below that of both PMMA and C1. Therefore, blends of C1 with PLA annealed in air or vacuum should exhibit a surface depletion of C1. However, if annealed in contact with water, surface enrichment will be controlled by the relative values of the interfacial tension of the polymers with water rather than air. Using the measured γ_p values, interfacial tensions of each polymer with water γ_{pw} were calculated. The comb γ_{pw} is significantly below that of PLA/water, suggesting a strong driving force for comb surface segregation upon water-based annealing.

XPS Analysis of Blend Surfaces. Surface compositions of PLA/C1 blend films were assessed by XPS. Spectra were deconvoluted as five component peaks representative of the bonding environments in the blend. To allow comparison between spectra, data before and after annealing were normalized to have equivalent *C*OO peak (∼289 eV) areas. Example raw data from high-resolution C_{1s} scans of two blends, 80:20 and 90:10 w:w PLA:C1, are shown in Figure 5 before and after annealing in water. Surface segregation of C1 upon annealing is indicated by the larger area contribution to the spectra at ∼286.5 eV, characteristic of EO carbon in the comb side chains. Figure 5 also plots this peak deconvoluted from the spectra before and after annealing.

The near-surface volume fraction of comb polymer ϕ^s_{comb} calculated from best fit XPS data for blends as-cast, after annealing in a vacuum at 120 °C for 4 days, and after annealing in water at 70 °C for 4 days are plotted vs ϕ^b_{comb} in Figure 6. Also plotted in Figure 6 is $\phi^s_{comb} = \phi^b_{comb}$ (dashed line), the expected surface composition if no surface

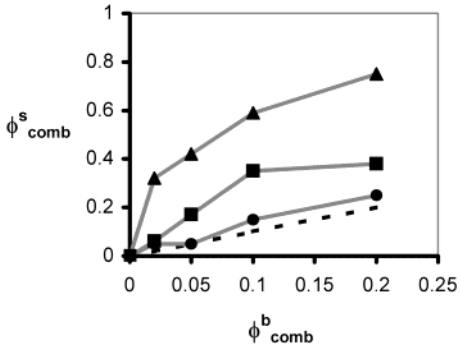

Figure 6. Surface segregation of comb polymer in PLA blends measured by XPS. (- - -) Expected surface composition for no segregation. (■) Surface volume fraction comb polymer calculated from XPS data for unannealed PLA/C1 blends. (▲) Surface volume fraction comb polymer for blends annealed 4 days at 70 °C in H_2O. (●) Surface volume fraction comb polymer for blends annealed 4 days in a vacuum at 120 °C.

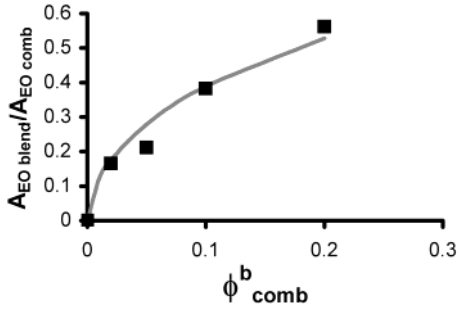

Figure 7. Comparison of experimental EO C_{1s} carbon peak areas with best-fit SCF predictions. $A_{EO\ blend}/A_{EO\ comb}$ is the ratio of the C_{1s} EO carbon peak (BE = 286.5 eV) in blends to that in a film of pure comb polymer. (■) XPS data. (═) Best fit using SCF concentration profiles for blend gives $\phi^{top1}_{comb} = 0.87$ for $\phi^b_{comb} = 0.20$.

enrichment or depletion occurs. As-cast samples show significant comb surface segregation. Blends annealed in a vacuum show a drop in ϕ^s_{comb} vs the as-cast condition to approximately the bulk concentration. Though the surface energy values in Table 4 suggest that a *depletion* of comb might be expected, entropic driving forces associated with the comb architecture may balance enthalpic effects.[57] In contrast, annealing blends in contact with water enhances comb surface segregation, as expected from interfacial energy considerations and SCF model predictions.

The ϕ^s_{comb} values measured by XPS are a weighted average of the comb composition within the top ∼50 Å of blends. To obtain an estimate of the comb concentration in the top 5−10 Å of the blends, SCF model concentration profiles were used to generate theoretical ratios of the ethylene oxide carbon C_{1s} peak in blends ($A_{EO\ blend}$) to that in the pure comb polymer ($A_{EO\ comb}$). Best fits to the experimentally measured $A_{EO\ blend}/A_{EO\ comb}$ ratios were obtained from SCF concentration profiles as described in the Experimental Section, with $\chi_{AS} = 1.25$, as shown in Figure 7. Concentration profiles corresponding to these best-fit $A_{EO\ blend}/A_{EO\ comb}$ ratios are shown in Figure 1. The SCF profiles for these parameters show a rapid decay of the comb concentration moving from the top layer of the blend into the bulk. Thus, SCF predicts a concentration of comb in the topmost surface layer $\phi^{top1}_{comb} \approx 0.90$ for $\phi^b_{comb} = 0.20$; surface coverage in the top layer is nearly complete for 20 vol % comb in the bulk.

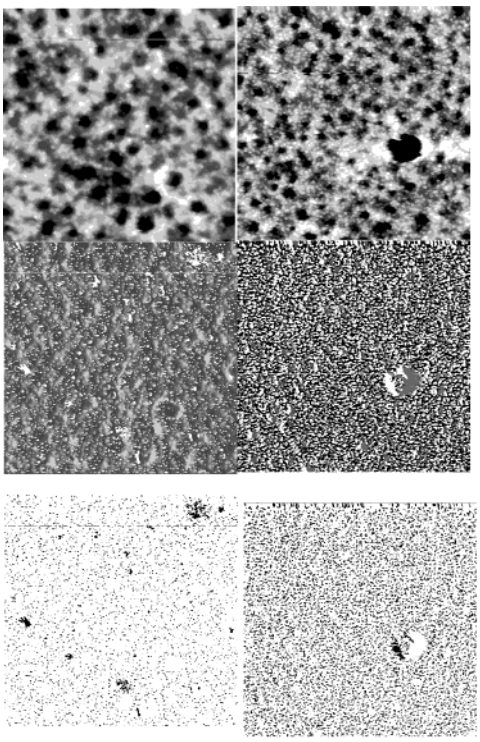

Figure 8. Representative AFM images of nanosphere-labeled PLA:C2:C2−RGD4 blends. Shown are 5 μm × 5 μm AFM scans of water-annealed blends. Images top to bottom are AFM topography, AFM phase, and the processed phase image binarized to depict the nanospheres only. Topography height gray scale range is 200 nm black to white and phase gray scale is 60°. Blend compositions are (w:w:w): (left) 80:19:1 blend; (right) 80:10:10 blend.

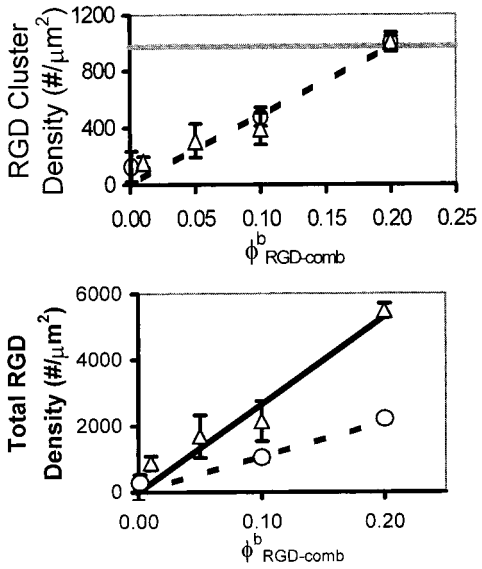

Figure 9. Peptide cluster density and total peptide density on surface-segregated blends. (a) Total cluster density for two cluster sizes, 5.44 peptides/comb (C2−RGD4, △) and 2.2 peptides/comb (C2−RGD2, ○). Gray line is maximum cluster density presented by pure RGD comb films; dashed line is linear best fit to cluster density data. (b) Total RGD density for the same two cluster sizes. The lines show best-fit trends expected for a rule of mixtures expression of C2−RGD2 or C2−RGD4 at the blend surface.

Surface Expression of Clustered RGD. Segregation of a mixture of unmodified and RGD-bearing combs allowed tunable nanoclustering of the adhesion ligand on blend surfaces. Blends were prepared with a fixed total concentration of comb polymer $\phi^{b}_{comb} = \phi^{b}_{unmodified} + \phi^{b}_{RGD-bearing} = 0.2$ and the relative ratio of unmodified to RGD-bearing comb was varied to control the total surface density of RGD achieved. RGD nanoclusters expressed at the surface of water-annealed blends were labeled with ∼30 nm diameter polystyrene spheres and imaged by AFM to determine the amount and spatial distribution of nanoscale RGD clusters at the surface.

Representative AFM topography and phase images are presented in Figure 8 for poly(L-lactide)/C2/C2−RGD4 blends containing 1 and 10 wt % C2−RGD4. The blends exhibited a pitted as-cast morphology due to spin-coating from a highly volatile solvent (chloroform), which persisted after annealing. AFM on noncrystalline poly(D,L-lactide)/comb blends had an identical morphology, ruling out an effect of crystalline-amorphous phase separation, and X_c values measured for as cast and annealed samples were only 5.2% and 19.2%, respectively. AFM phase data, depending on the sample under investigation, displays contrast arising from chemical or stiffness variations near the sample surface.[70−74] Thus, the PS nanospheres ($T_g \sim 100$ °C), which are significantly stiffer than the blend at room temperature, are clearly defined in these images. Bright objects identified as the nanospheres in the phase images correlate with objects in the topography images of ∼30 nm height. (Unlabeled films exhibited a surface rms roughness outside of the pits of ∼5 nm). The blends exhibit immobilized nanospheres both on the surface of the films and within pits (those large enough for the AFM tip to effectively probe), indicating that the comb polymer is uniformly present in the exterior surface layer of these rough blend films. The high contrast between the labels and underlying blend surface facilitated analysis through binarization of the phase images as shown in Figure 8**.** Cluster and total RGD surface densities as a function of bulk RGD comb concentration determined from AFM images are plotted in Figure 9.

Three conclusions are drawn from the labeling results. First, despite the uncertainty in label density caused by the pitted topography of the films, the cluster density data is consistent with the predicted quasi-2D conformation of the comb polymer in the top surface layer, similar to that seen on pure comb films.[1] If comb chains at the surface took on Gaussian conformations with extensive chain interpenetration, RGD cluster labeling would saturate at low bulk RGD comb concentrations, $\phi^{b}_{RGD-comb} \sim 0.05$, due to the large number ($\sim N^{1/2}$) of chains contributing to the surface layer per R_g^2 surface area. Instead, Figure 9 shows that the surface label density increases with $\phi^{b}_{RGD-comb}$ up to 0.2. Second, the cluster density at $\phi^{b}_{RGD-comb} = 0.2$ (∼950 clusters/μm^2) is comparable to the maximum cluster density measured on pure RGD comb films, in agreement with the combined XPS/SCF analysis indicating near-complete top surface layer coverage of the blend at this bulk composition. Third, the RGD-modified and unmodified combs appear proportionally co-segregated to the surface. The measured cluster densities appear linear between $\phi^{b}_{RGD-comb} = 0$ and the maximum density at $\phi^{b}_{RGD-comb} \sim 0.20$. Equal co-segregation of unmodified and functionalized combs is also indicated by comparing surface densities of 5.4 RGD and 2.2 RGD combs,

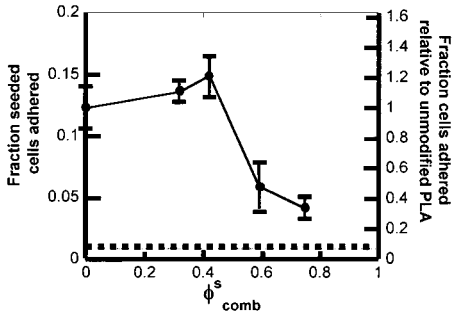

Figure 10. Adhesion of WTNR6 fibroblasts to PLA/C1 blends after 24 h vs the surface volume fraction of comb polymer ϕ^s_{comb} in water-annealed PLA/comb blends. The dashed line is the previously measured cell resistance of pure comb films.

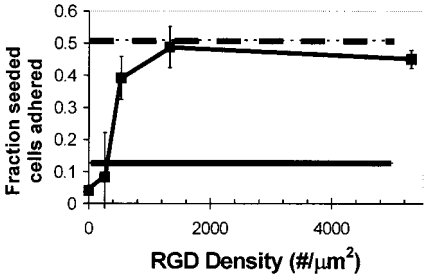

Figure 11. Cell adhesion on PLA/C2/C2−RGD4 blends with increasing RGD content. Comparison of WTNR6 fibroblast adhesion at 24 h on blends with surface RGD expression: (···) mean fraction seeded cells adhered on TCPS control substrates and (−) an unmodified PLA control.

which showed the same RGD surface density when equivalent bulk RGD comb concentrations were present.

Disklike conformations for the comb chains in the top layer of a segregated film imply that the diameter of peptide clusters at the surface will be sensitive to the molecular weight of the comb polymer. Increasing the comb molecular weight should not only increase segregation, as indicated by SCF calculations, it should also increase the radius of peptide nanoclusters presented in the top layer. Thus, by controlling functionalization of the comb copolymer, molecular weight, and the amount of comb used, the three main physical parameters of the surface structure (number of peptides per nanocluster, nanocluster diameter, and total coverage) can be tailored to specific applications.

Cell Attachment Studies. Surface segregation of comb polymer can be used to control cell adhesion on PLA devices. Fibroblast attachment to PLA in serum-containing media is substantially reduced through surface segregation of comb polymer. Figure 10 shows the fraction of seeded cells adhered and fraction cells adhered relative to unmodified PLA as a function of the near-surface comb volume fraction ϕ^s_{comb} determined by XPS. Cell attachment is inversely correlated with comb surface enrichment, but a minimum $\phi^s_{comb} = 0.50$ appears necessary to reduce cell attachment. The fraction of cells attaching to blends with $\phi^b_{comb} = 0.20$ is not as low as measured for pure comb polymer films,[1] however, the absolute cell number on these surfaces after 24 h is less than 5% of the total seeded.

Co-segregation of RGD-modified combs allows cell adhesion to be tuned on PLA blends. Figure 11 plots the fraction of seeded fibroblasts attached vs the surface density of RGD

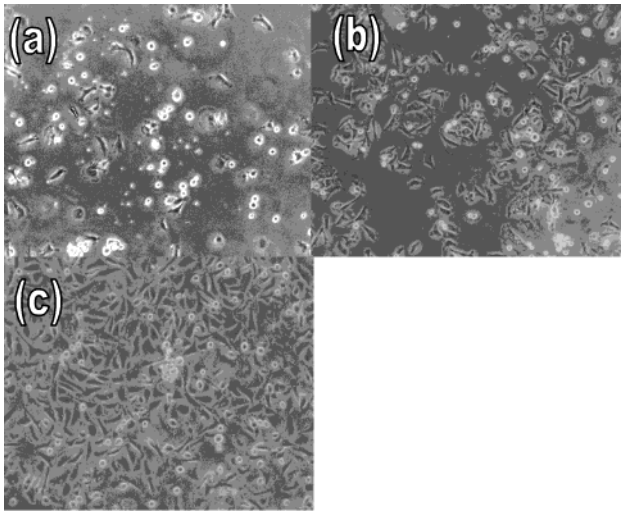

Figure 12. Phase contrast micrographs of cell morphology for comb/PLA blends at 24 h. (a) 80:19:1 w:w:w PLA:C1:C1−RGD1. (b) 80:18:2 PLA:C1:C1−RGD1. (c) 80:15:5 PLA:C1:C1−RGD1.

on annealed blends. Cell attachment saturates at a level comparable to that seen on highly adhesive TCPS controls for only 5 wt % C2−RGD4 in the bulk due to co-segregation of the RGD comb. In addition, RGD-expressing surfaces supported much greater cell attachment than unmodified PLA. As shown in Figure 12, after 24 h annealing in water the surface density of RGD was sufficient to promote attachment and spreading of cells on the comb-modified blend. Further annealing did not increase the adhesivity of the surfaces (data not shown).

Cell attachment on RGD-expressing PLA blends was mediated by specific RGD−integrin interactions. Addition of 85 μM soluble GRGDSP to the media promoted rapid rounding of the cells and over 4 h, >90% cell detachment, indicating that integrin−RGD interactions were the adhesion-promoting linkages between cells and the surfaces. Changing to fresh media after exposure to soluble RGD (before complete detachment), cells were able to respread on the tethered ligand blend surfaces. Thus, by addition of 20 wt % comb to PLA and water annealing, integrin-mediated cell adhesion can be controlled at the blend surface, augmenting the favorable bulk mechanical and degradation properties of this biomaterial.

Degradation Kinetics of Comb/PLA Blends. A critical issue in the use of surface segregation for tissue engineering is the stability of the surface layer. Degradation of the system must be slow enough to allow cell behavior to be guided for an appropriate time period by the ligand-bearing surface. This is especially important since the comb is amphiphilic and will improve the ability of water to penetrate the bulk of the blend as it degrades. Ligand can be lost from the degrading blend surface through either hydrolysis of the ester linkage between the RGD peptide and comb polymer, or via degradation-induced solubilization of surface-localized comb polymer. The time course of ligand loss from surface-segregated 80:20 w:w PLA:C2−RGD2 blends was followed by monitoring the release of fluorescent nanosphere-labeled RGD peptides from thin films degraded under physiological conditions, as shown in Figure 13. Ligand density at the

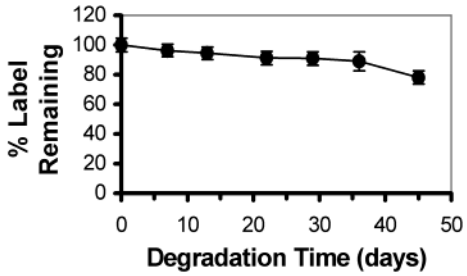

Figure 13. Labeled ligand loss from the surface of PLA/C2−RGD2 blends over time under physiological conditions.

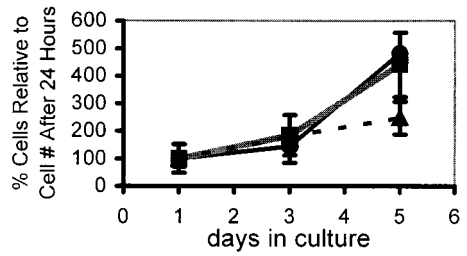

Figure 14. RGD-bearing PLA blends support cell attachment and growth over several days in culture. WTNR6 fibroblasts were seeded on PLA/C2/C2−RGD3 containing (●) 615 RGD/μm^2, (■) 880 RGD/μm^2, or (▲) 1760 RGD/μm^2. Cell number was measured after 24, 72, and 120 h in culture.

surface of the blend decreased slowly under physiological conditions, retaining >90% of the labeled ligand after 3 weeks incubation in saline.

As a practical measure of short-term surface stability, we also assessed the ability of RGD-bearing PLA surfaces to support sustained cell attachment and growth of WTNR6 fibroblasts over 5 days in culture. The expansion of cells over this time period on surfaces presenting three different densities of RGD peptide is shown in Figure 14. At the end of this culture period, addition of 85 μm soluble GRGDSP to media of cells cultured on 1760 RGD/μm^2 C2−RGD3 blends promoted detachment of >90% of the attached cells, indicating peptide-mediated adhesion even after several days in culture. Successful expansion of cells on these surfaces thus indicates stability of the tethered RGD surface over this time frame.

The use of a methacrylate backbone for the comb polymer means that the additive will not itself be biodegradable. The hydrolytic stability of the comb may be key for maintaining the protein-resistance and ligand-presentation properties of the blend surface for reasonable time periods. However, as the matrix degrades in the long-term, the remaining comb polymer may not be problematic. Methacrylates are well tolerated in contact with tissue (e.g., as bone sealants or intraocular lenses) and thus residual comb additive may not provoke undue inflammation in vivo. In addition, poly(ethylene glycol) is known to be cleared by the renal system[8] and thus residual amphiphilic comb may also be removed from the body in a similar nondetrimental manner. It remains for future work to determine whether fully degradable comb polymers can provide similar surface properties over the required time frame for guiding cell function in tissue engineering applications.

Conclusions

The results of these studies suggest surface segregation of peptide-modified P(MMA-*r*-POEM) as an attractive approach to creating nanoscale ligand clusters on the surface of bioresorbable devices. SCF studies and cluster density measurements indicate that combs exhibit quasi-2D conformations at the blend−water interface, similar to findings for pure comb polymer/water interfaces.[1] Ligand clustering at the blend surface should thus be highly effective, since all ligands attached to combs in the top molecular layer of film are made accessible to cells. Cluster size and density can consequently be controlled by the molecular weight and number of ligands per modified comb, as well as the ratio of ligand-bearing to unmodified comb in the blend. While cell resistance of blends incorporating only unmodified comb was somewhat below that of the pure comb polymer, this might be improved by the use of slightly longer PEO side chains.[1,72] More work is needed to assess the optimum comb geometry to encourage receptor clustering but discourage nonspecific protein adsorption.

As a fabrication method, surface segregation is readily adapted to current scaffold manufacturing routes and could be readily achieved by simply incorporating a water-annealing step within phase separation,[30] particulate leaching,[11,12] or phase-inversion casting[9,27,75] fabrication methods. In contrast to line-of-sight coating methods for which the modification of interior scaffold pores is problematic, surface segregation effectively modifies all surfaces of complex three-dimensional scaffolds. One important and as yet unresolved issue is whether small fractions of nondegradable combs incorporated into tissue engineering devices will affect the viability of the device in vivo. Preliminary studies using combs with hydrolyzable backbones have shown that the comb segregation strategy is generalizable to other backbone chemistries, and current efforts are underway to develop a reliable synthetic route to such materials.[76,77]

Acknowledgment. We gratefully acknowledge Prof. M. F. Rubner for access to the contact angle apparatus, and the assistance of Catherine Reyes in obtaining the degradation data. This work made use of MRSEC Shared Experimental Facilities supported by the National Science Foundation under Award No. DMR98-08941. This work was supported in part by the Whitaker Foundation Grant No. RG-97-0196, NSF Award No. DMR98-17735, and NIH 1R0GM59870-01.The authors acknowledge the support of NIST, U.S. Department of Commerce, in providing neutron facilities used in this work. This material is based upon activities supported by the National Science Foundation under Award No. DMR-9986442.

References and Notes

(1) Irvine, D. J.; Mayes, A. M.; Griffith, L. G. *Biomacromolecules* **2001**, *2*, 85.
(2) Banerjee, P.; Irvine, D. J.; Mayes, A. M.; Griffith, L. G. *J. Biomed. Mater. Res.* **2000**, *50*, 331.
(3) Massia, S. P.; Hubbell, J. A. *J. Cell Biol.* **1991**, *114*, 1089.
(4) Roberts, C.; Chen, C. S.; Mrksich, M.; Martichonok, V.; Ingber, D. E.;Whitesides, G. M. *J. Am. Chem. Soc.* **1998**, *120*, 6548.
(5) Pettit, D. K.; Gombotz, W. R. *TIB Technol.* **1998**, *16*, 343.
(6) Mathiowitz, E.; Jacob, J. S.; Jong, Y. S.; et al., *Nature* **1997**, *386*, 410.

(7) Saltzman, W. M. *MRS Bull.* **1996**, *21*, 62.
(8) Lanza, R. P.; Langer, R.; Chick, W. L. *Principles of Tissue Engineering*; R. D. Landes Company: Georgetown, TX, 1997.
(9) Liu, D.-M.; Dixit, V. *Porous Materials for Tissue Engineering*; Trans Tech Publications: Ütikon-Zürich, Switzerland, 1997.
(10) Park, A.; Wu, B.; Griffith, L. G. *J. Biomater. Sci., Polym. Ed.* **1998**, *9*, 89.
(11) Peter, S. J.; Miller, M. J.; Yasko, A. W.; Yaszemski, M. J.; Mikos, A. G. *J. Biomed. Mater. Res.* **1998**, *43*, 422.
(12) Wake, M. C.; Gupta, P. K.; Mikos, A. G. *Cell Transp.* **1996**, *5*, 465.
(13) Peters, M. C.; Mooney, D. J. *Mater. Sci. Forum* **1997**, *250*, 43.
(14) Vacanti, C. A.; Kim, W.; Upton, J.; Vacanti, M. P.; Mooney, D.; Schloo, B.; Vacanti, J. P. *Transplant Proc.* **1993**, *25*, 1019.
(15) Wilkins, L. M.; Watson, S. R.; Prosky, S. J.; Meunier, S. F.; Parenteau, N. L. *Biotechnol. Bioeng.* **1994**, *43*, 747.
(16) Yannas, I. V. *Bioartificial Organs* **1997**, *831*, 280.
(17) Yannas, I. V.; Lee, E.; Orgill, D. P.; Skrabut, E. M.; Murphy, G. F. *Proc. Natl. Acad. Sci. U.S.A.* **1989**, *86*, 933.
(18) Ellis, D. L.; Yannas, I. V. *Biomaterials* **1996**, *17*, 291.
(19) Bellamkonda, R.; Aebischer, P. *Biotechnol. Bioeng.* **1994**, *43*, 543.
(20) Spilker, M. H.; Yannas, I. V.; Hsu, H. P.; Norregaard, T. V.; Kostyk, S. K.; Spector, M. *Tissue Eng.* **1997**, *3*, 309.
(21) Chamberlain, L. J.; Yannas, I. V.; Arrizabalaga, A.; Hsu, H. P.; Norregaard, T. V.; Spector, M. *Biomaterials* **1998**, *19*, 1393.
(22) Cieslinski, D. A.; Humes, H. D. *Biotechnol. Bioeng.* **1994**, *43*, 678.
(23) Niklason, L. E.; Gao, J.; Abbott, W. M.; H. K. K.; Houser, S.; Marini, R.; Langer, R. *Science* **1999**, *284*, 489.
(24) Uyama, S.; Kaufmann, P. M.; Tadeka, T.; Vacanti, J. P. *Transplantation* **1993**, *55*, 932.
(25) Wake, M. C.; Patrick, C. W.; Mikos, A. G. *Cell Transp.* **1994**, *3*, 339.
(26) Lyman, D. J.; Rowland, S. M. In *Encyclopedia of Polymer Science and Engineering*; Mark, H. F., Kroschwitz, J. I., Eds.; Wiley: New York, 1985; Vol. 2, p 267.
(27) Thomson, R. C.; Wake, M. C.; Yaszemski, M. J.; Mikos, A. G. In *Biopolymers II*; Peppas, N. A., Langer, R. S., Eds.; Springer-Verlag: New York, 1995; Vol. 122, p 245.
(28) Hubbell, J. A.; Massia, S. P.; Desai, N. P.; Drumheller, P. D. *Bio/Technology* **1991**, *9*, 568.
(29) Schugens, C.; Maquet, V.; Grandfils, C.; Jerome, R.; Teyssie, P. *J. Biomed. Mater. Res.* **1996**, *30*, 449.
(30) van de Witte, P.; Esselbrugge, H.; Dijkstra, P. J.; van den Berg, J. W. A.; Feijen, J. *J. Mem. Sci.* **1996**, *113*, 223.
(31) Whang, K.; Thomas, C. H.; Healy, K. E.; Nuber, G. *Polymer* **1995**, *36*, 837.
(32) Bearinger, J. P.; Castner, D. G.; Healy, K. E. *J. Biomater. Sci., Polym. Ed.* **1998**, *9*, 629.
(33) Drumheller, P. D.; Elbert, D. L.; Hubbell, J. A. *Biotech. Bioeng.* **1994**, *43*, 772.
(34) Maheshwari, G.; Brown, G.; Lauffenburger, D. A.; Wells, A.; Griffith, L. G. *J. Cell. Sci.* **2000**, *113*, 1677.
(35) Barrera, D. A.; Zylstra, E.; Lansbury, P. T.; Langer, R. *Macromol.* **1995**, *28*, 425.
(36) Ouchi, T.; Fujino, A.; Tanaka, K.; Banba, T. *J. Controlled Release* **1990**, *12*, 143.
(37) Black, F. E.; Hartshorne, M.; Davies, M. C.; et al. *Langmuir* **1999**, *15*, 3157.
(38) Scheutjens, J. M. H. M.; Fleer, G. J. *J. Phys. Chem.* **1979**, *83*, 1619.
(39) Evers, O. A.; Scheutjens, J. M. H. M.; Fleer, G. J. *Macromolecules* **1990**, *23*, 5221.
(40) Fleer, G. J.; Cohen Stuart, M. A.; Scheutjens, J. M. H. M.; Cosgrove, T.; Vincent, B. *Polymers at Interfaces*; University Press: Cambridge, U.K., 1993.
(41) Eguiburu, J. L.; Iruin, J. J.; Fernandez-Berridi, M. J.; Roman, J. S. *Polymer* **1998**, *39*, 6891.
(42) Nijenhuis, A. J.; Colstee, E.; Grijpma, D. W.; Pennings, A. J. *Polymer* **1996**, *37*, 5849.
(43) Schantz, S. *Macromolecules* **1997**, *30*, 1419.
(44) Utracki, L. A. *Polymer Alloys and Blends: Thermodynamics and Rheology*; Hanser Publishers: New York, 1990.
(45) Barton, A. F. M. *CRC Handbook of Polymer-Liquid Interaction Parameters*; CRC Press: Boca Raton, FL, 1990.
(46) Reed, A. M.; Gilding, D. K. *Polymer* **1981**, *22*, 494.
(47) Iannace, S.; Nicolais, L. *J. Appl. Polym. Sci.* **1997**, *64*, 911.
(48) Balta-Calleja, F. J. *X-ray Scattering of Synthetic Polymers*; Elsevier: New York, 1989.
(49) Sarasua, J.-R.; Prud'homme, R. E.; Wisniewski, M.; Le Borgne, A.; Spassky, N. *Macromolecules* **1998**, *31*, 3895.
(50) Wu, S. *Polymer Interface and Adhesion*; Marcel Dekker: New York, 1982.
(51) Girifalco, L. A.; Good, R. J. *J. Phys. Chem.* **1957**, *61*, 904.
(52) Good, R. J. In *Treatise on Adhesion and Adhesives*; Patrick, R. L., Ed.; Marcel Dekker, Inc.: New York, NY, 1967; Vol. 1, p 9.
(53) Beamson, G.; Briggs, D. *High-Resolution XPS of Organic Polymers*; Wiley: New York, 1992.
(54) Shard, A. G.; Davies, M. C.; Tendler, S. J. B.; Nicholas, C. V.; Purbrick, M. D.; Watts, J. F. *Macromolecules* **1995**, *28*, 7855.
(55) Smith, G. C. *Quantitative Surface Analysis for Materials Science*; Institute of Metals, Brookfield, VT, 1991.
(56) Clark, D. T.; Thomas, H. R. *J. Polym. Sci. Polym. Chem.* **1977**, *15*, 2843.
(57) Walton, D. G.; Mayes, A. M. *Phys. Rev. E* **1996**, *54*, 2811.
(58) Fredrickson, G. H. *Macromolecules* **1996**, *29*, 7919.
(59) Gersappe, D.; Irvine, D.; Balazs, A. C.; Liu, Y.; Sokolov, J.; Rafailovich, M.; Schwarz, S.; Pfeiffer, D. G. *Science* **1994**, *265*, 1072.
(60) T_g of the comb polymer was determined by group contribution calculations according to the method of Van Krevelen: *Properties of Polymers*; Elsevier: New York, 1990.
(61) Alegria, A.; Colmenero, J.; Ngai, K. L.; Roland, C. M. *Macromolecules* **1994**, *27*, 4486.
(62) Ferry, J. D. *Viscoelastic Properties of Polymers*; Wiley: New York, 1980.
(63) Yamaguchi, M.; Miyata, H. *Macromolecules* **1999**, *32*, 5911.
(64) Han, C. D.; Jhon, M. S. *J. Appl. Polym. Sci.* **1986**, *32*, 3809.
(65) Han, C. D.; Kim, J. K. *Macromolecules* **1989**, *22*, 4292.
(66) Alamo, R. G.; Graessley, W. W.; Krishnamoorti, R.; Lohse, D. J.; Londono, J. D.; Mandelkern, L.; Stehling, F. C. *Macromolecules* **1997**, *30*, 561.
(67) Londono, J. D.; Wignall, G. D. *Macromolecules* **1997**, *30*, 3821.
(68) Walton, D. G.; Soo, P. P.; Mayes, A. M.; et al. *Macromolecules* **1997**, *30*, 6947.
(69) Park, A.; Griffith Cima, L. *J. Biomed. Mater. Res.* **1996**, *31*, 117.
(70) Burnham, N. A.; Behrend, O. P.; Oulevey, F.; et al. *Nanotechnology* **1997**, *8*, 67.
(71) Chen, X.; McGurk, S. L.; Davies, M. C.; et al. *Macromolecules* **1998**, *31*, 2278.
(72) Van Noort, S. J. T.; Van der Werf, J. O.; De Grooth, B. G.; Van Hulst, N. F.; Greve, J. *Ultramicroscopy* **1997**, *69*, 117.
(73) Magonov, S. N.; Elings, V.; Whangbo, M. H. *Surf. Sci.* **1997**, *375*, L385.
(74) Schmitz, I.; Schreiner, M.; Friedbacher, G.; Grasserbauer, M. *Appl. Surf. Sci.* **1997**, *115*, 190.
(75) Hester, J. F.; Banerjee, P.; Mayes, A. M. *Macromolecules* **1999**, *32*, 1643.
(76) Mayes, A. M.; Irvine, D. J.; Griffith, L. G. *Mater. Res. Soc. Symp. Proc.* **1998**, *530*, 73.
(77) Winblade, N. D.; Nikolic, I. D.; Hoffman, A. S.; Hubbell, J. A. *Biomacromolecules* **2000**, *1*, 523.

BM015510F